# ALOS-PALSAR performances on a multiple sensor DInSAR scenario for deformation monitoring

Pablo Blanco, Roman Arbiol and Vicenç Palà
Remote Sensing Department
Institut Cartogràfic de Catalunya (ICC)
Parc de Montjuïc, s/n, 08038 Barcelona, Spain
pablo.blanco@icc.cat

*Abstract*—**The Institut Cartogràfic de Catalunya (ICC) has developed its own DInSAR processing chain during the past years. Initial topographic interferometry applications have evolved into Multi Image Differential Interferometry (MI DInSAR) for terrain deformation monitoring purposes. The appearance of the JAXA's L-band sensor ALOS-PALSAR opens new possibilities to increase the amount of useful information which serve as input to these techniques and brings complementarity to the already successful C-band missions as ESA's ERS and ENVISAT. In the frame of deformation monitoring, PALSAR benefits and L-C band combination strategies are here investigated. L-band coherence enhancement in rural areas is addressed, allowing information retrieval on areas that would be inaccessible at C-band. Furthermore, PALSAR polarimetric channels combination is investigated in order to increase the number of pixels from whom deformation values can be extracted. Deformation results employing PALSAR and ENVISAT data are presented.**

***Coherence, DInSAR, polarimetry, subsidence, terrain deformation***

## I. INTRODUCTION

During the past years, Multiple Images DInSAR (MI DInSAR) techniques have been widely developed [1-4] revealing to be a reliable tool for deformation monitoring. These techniques are able to provide the temporal deformation pattern of the studied area minimizing the effects of atmospheric artifacts. The upcoming of new SAR sensors expands MI DInSAR capabilities towards a more complete characterization of the motion information of the studied area.

In particular, L band ALOS-PALSAR present two important features which can be foreseen as complementary to the existent list of SAR sensors. These are its 1280 MHz working frequency and its polarimetric capabilities. Keeping in mind the final scope of retrieving temporal deformation from the studied areas, ALOS-PALSAR benefits and combining strategies with other band working sensors are here investigated. A test area where different deformation phenomena are taken place has been chosen. Correspondingly, a stack of PALSAR and ASAR interferograms have been created and different tests have been done among them. The employed data is described in section II.

Scattering mechanism depend, among others, on the wavelength of the employed signal. This makes L-band especially interesting over vegetated areas as, in opposition to C-band, penetration allows to study the underneath canopy surface behaviour. In coherence terms this should provoke a coherence improvement and access to non coherent areas in C-band images. In order to validate this, coherence performances are studied over the PALSAR and ASAR stacks. Therefore, when moving into a MI DInSAR frame, an increment of the number of useful points should be expected. This study is performed in section III.

Two types of deformation movements are selected for motion detectability comparison. PALSAR and ASAR fringes corresponding to a wide and strong (30 cm/y) subsidence movement are compared. Furthermore, a long term (2 cm/y) and localized subsidence movement is studied. Here, the ICCs MI DInSAR processor will be applied to the PALSAR and ASAR stacks. Comparison in terms of number of useful points and deformation behavior from both datasets are addressed in section V.

PALSAR is capable to provide full polarimetric images. The employed PALSAR stack accounts for HH and HV images. Therefore, efforts are addressed to take profit of both channels to increase the density of useful pixels. Employing coherence as a scattering stability indicator, a HH and HV channel combination on the stack of interferograms is also proposed and the corresponding deformation map is presented.

Finally, conclusions and future work are exposed in section VI.

## II. AVAILABLE DATA

The test area (in yellow) is located in the Bages region in Catalonia (Spain) as depicted in Fig.1. The ALOS-PALSAR FBS and FBD coverage corresponds to path 660 and frames 820 and 830 (from south to north correspondingly, in black). The ENVISAT-ASAR coverage corresponds to track 244 and frame 837 (in green). In this area, several deformation episodes have been reported, mainly caused by mining activities.

The spatiotemporal distribution of the PALSAR and ASAR interferogram stack are shown in Fig.2 and Fig.3 respectively. The nodes represent the images and the arcs, the interferograms. The ASAR stack is composed of 43 interferograms out of 13 images with a maximum spatial baseline of 300 m.

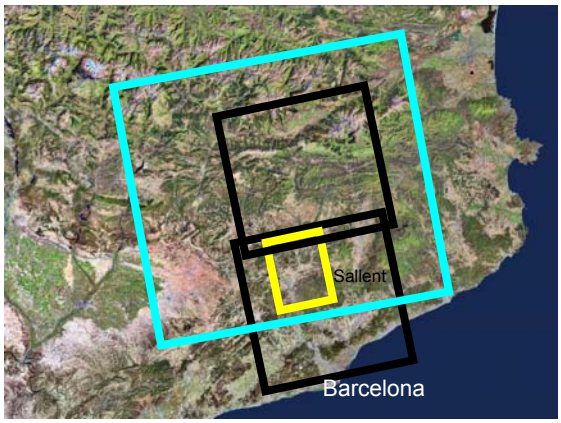


Figure 1. Selected test area (yellow). PALSAR (black) and ASAR (green) footprints.

The PALSAR stack is composed of 10 interferograms out of 2 FBS images (green) and 5 FBD (red) images, with a maximum spatial baseline of 1200m. It is worth noting that the number of interferograms and the temporal coverage of both data sets is not the same. A selection on the ENVISAT data could be done so only those [2007,2008] images and their corresponding interferograms (in correspondence to PALSAR) had been included in the phase analysis. Nevertheless, it has been preferred to take profit of the whole dataset so a more reliable statistic is at least available for ASAR.

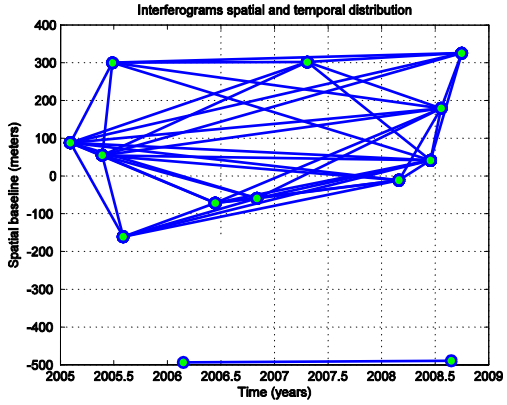


Figure 2. ASAR interferograms distribution.

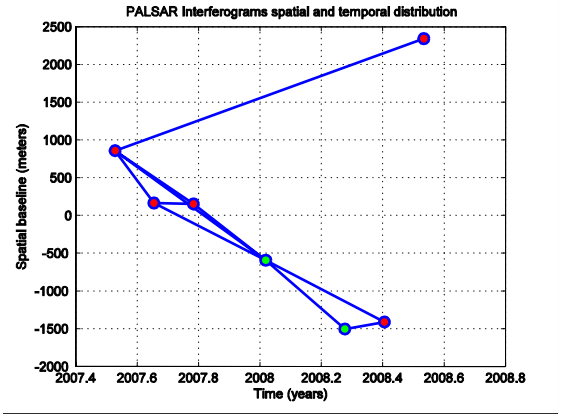


Figure 3. PALSAR interferograms distribution.

## III. C BAND VS. L BAND. COHERENCE BEHAVIOUR

Employing the described ASAR and PALSAR (HH channel) interferograms stacks, their mean coherence maps are computed over the area of interest (Figs. 4 and 5 respectively). The studied area comprises both urban and rural areas. In black, the city of Sallent has been marked.

According to the results, PALSAR coherence is significantly increased in the rural areas compared to the ASAR coherence map. Urban areas remain coherent for both sensors. As commented, both temporal distributions are different and the ASAR set includes larger temporal baselines interferograms. Therefore, temporal decorrelation may be higher in the ASAR set. Nevertheless, when comparing mean coherence maps from similar periods and temporal baselines, the aforementioned behaviour is also reproduced.

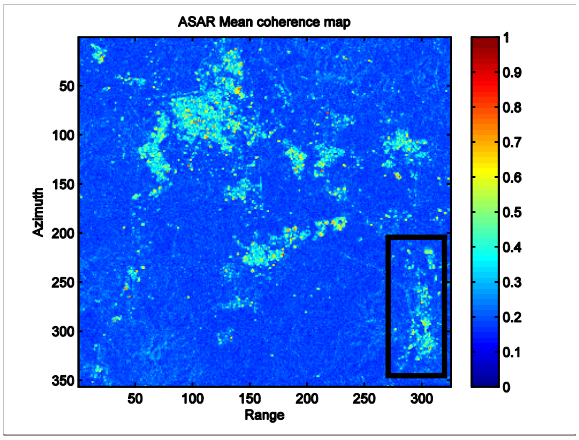


Figure 4. ASAR mean coherence map.

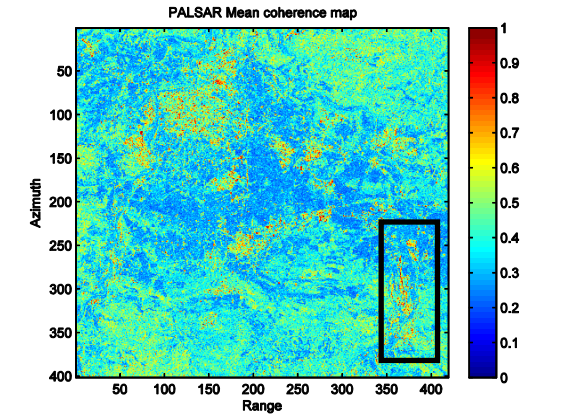


Figure 5. PALSAR mean coherence map.

The histograms of the mean coherence maps are computed and depicted in Fig.6. Here, PALSAR histograms are computed separately employing the HH and the HV interferograms. Confirming the mean coherence maps results, PALSAR coherence values are higher than ENVISAT's. Furthermore, HH channel is slightly higher than HV.

From these results, two main conclusions can be extracted. First, L band brings coherent information in areas where C band does not. Second, both HH and HV channels are

comparable in terms of phase quality, so strategies should be developed to combine both channels for deformation extraction purposes.

To confirm the obtained results, more PALSAR images are demanded, so further tests will be done in the future.

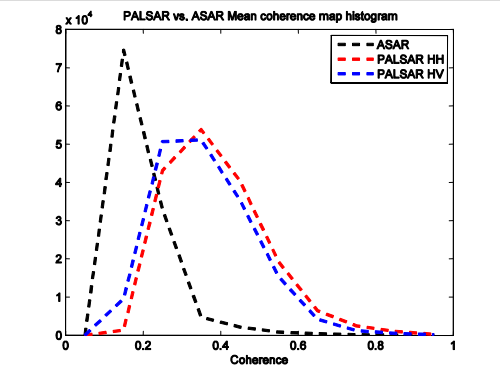


Figure 6. ASAR (black) and PALSAR (HH in red and HV in blue) mean coherence maps histograms.

## IV. DInSAR RESULTS

In the test area, fast and extensive movements were detected in previous studies (references) employing ASAR images, caused by subterranean mining works in the area. These are significant enough to be clearly detectable despite of the atmospheric artefacts. Nevertheless, as they are located at vegetated areas, PALSAR phase is investigated to test quality enhancement where C band fringes were masked.

Picked out of the PALSAR and ASAR interferograms stacks, two 2008 PALSAR interferograms of the deformation area are depicted Fig.7 in the upper row (46 days and 92 days temporal baselines). ENVISAT highest quality interferograms in 2008 are depicted in the lower row (35 days and 105 days temporal baseline). The detected movement magnitude is larger than 30 cm/year PALSAR fringes are better defined than ASAR, so the area monitoring can be improved by combining both sources of information.

## V. MI DInSAR DEFORMATION RESULTS

Once frequency impact on coherence has been investigated, deformation results on both ASAR and PALSAR data are obtained.

MI DInSAR is only applied to those quality pixels selected on the stack of interferograms. This selection is performed applying a mean coherence threshold value. Consequently, it is expected to select points in the PALSAR stack that would not be selected in the SAR one.

The city of Sallent presents a long-term subsidence movement in one of its neighbourhoods, caused by salt dissolution. ASAR and PALSAR HH stacks are processed with the ICC MI DInSAR algorithm. Pixel size is approximately 30 m x 30 m. The selected points are those whose mean coherence value exceeds 0.4 in ASAR and 0.55 in PALSAR. Due to the lower number of PALSAR interferograms coherence threshold is higher to ensure quality deformation results.

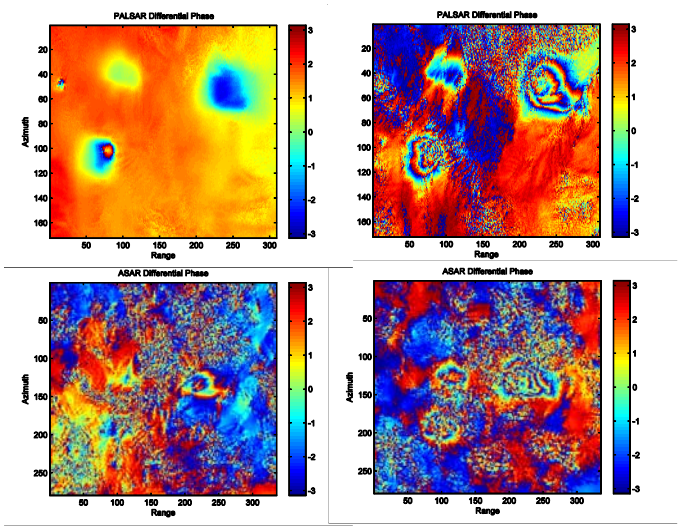


Figure 7. Deformation fringes (> 30 cm/year) generated by mine activities seen by PALSAR (first row) and ASAR (second row).

ASAR and PALSAR geocoded linear velocity maps of Sallent are depicted in Fig. 8 (left and right correspondingly). Even though it is possible to retrieve temporal series from PALSAR, the low number of images has prevented to do so.

Taking PALSAR quantities as approximate (due to the low number of images and interferograms employed) and assuming that temporal spans are not identical, two main conclusions can be extracted. In general, deformation behaviour is similar, whereas PALSAR allows access to C-band non-coherent areas (marked in black), which is helpful to give deformation interpretation.

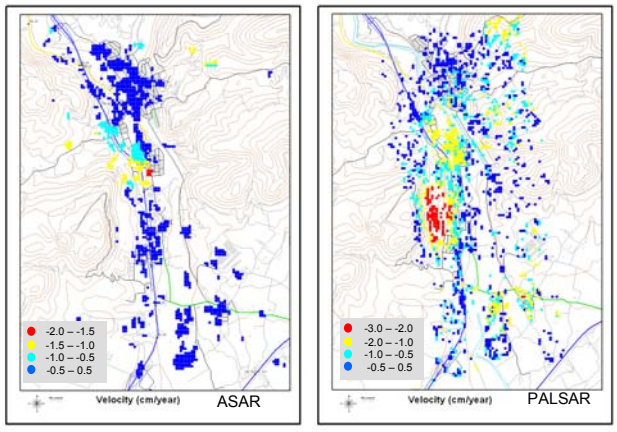


Figure 8. Linear velocity map of Sallent obtained from the ASAR stack (right) and thr PALSAR stack (left).

### *A. Polarimetry combination for coherent points enhacement*

In order to take profit of both ALOS HH and HV channels a strategy is proposed. The objective is to increase the number of useful points where deformation information could be extracted. Due to the difficulty of directly combining both polarization interferograms (risk to take a different phase centre as a deformation) two coherent pixels masks are created.

Pixels that exceed the proposed threshold and whose mean HH coherence is larger than HV are stored apart and vice-versa. HH selected pixels map is depicted in Fig.9, while HH>HV mask is depicted in Fig.10 and HH<HV mask in Fig.11.

A high coherence value will indicate a constant polarimetric mechanism from one image to the other. Therefore, the corresponding decorrelation factor will be low and the movement phase component will come out independently of the polarization channel.

Afterwards, MI DInSAR algorithm is applied to the HH stack for the HH>HV pixels map and to the HV stack for the HV>HH mask. Then, both linear velocity maps are summed up, as shown for the town of Sallent in Fig.12. Comparing this with the previous one (Fig.8) it can be said that in general the same motion pattern is obtained, but most important is that the final number of useful pixels is increased against the single channel case (10169 (HH) < 9078 (HH>HV)+ 4666 (HV>HH)). Again, more images are needed to extract more solid conclusions.

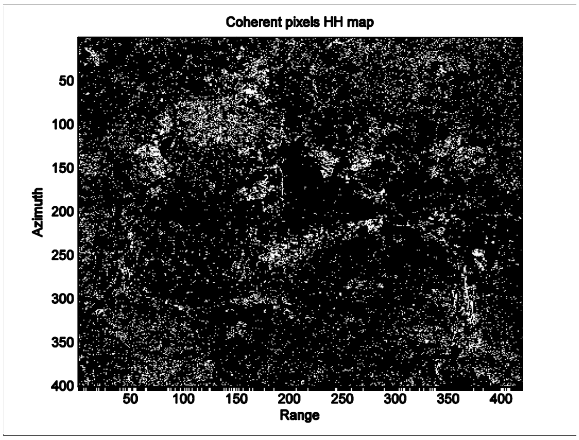


Figure 9. Selected pixels map from PALSAR HH stack.

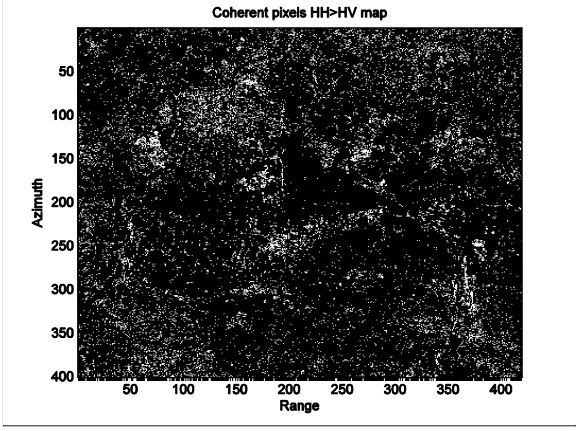


Figure 10. Selected pixels are those whose mean coherence is higher in the HH stack than in the HV stack.

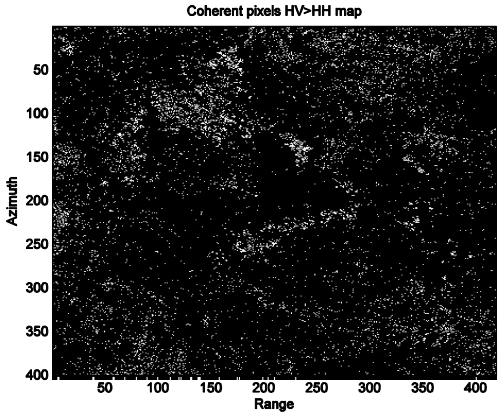


Figure 11. Selected pixels are those whose mean coherence is higher in the HV stack than in the HH stack.

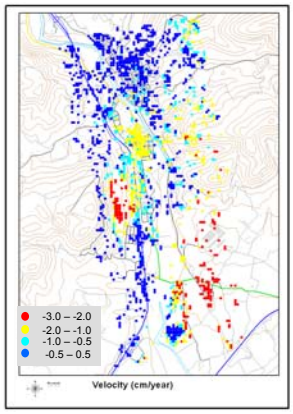


Figure 12. Linear velocity map of the city of Sallent combining HH and HV channels.

## VI. CONCLUSIONS

ALOS-PALSAR performances for deformation monitoring have been investigated. L-band coherence enhancements (mainly in rural areas) as well as its polarimetric capabilities lead to an increment of useful points and, therefore, access to new deformation information. In this sense, L and C band results have to be envisaged as complementary. More PALSAR images are needed to extend these studies. Combination optimization of the polarimetric channels as well as the L and C (and X) band data represents a mandatory issue for a more complete deformation monitoring characterization.


## ACKNOWLEDGMENTS

This work has been sponsored by JAXA and ESA under ALOS ADEN AOALO.3655


## REFERENCES


[1] Pablo Blanco-Sanchez, Jordi J. Mallorquí, Sergi Duque, and Daniel Monells, "The Coherent Pixels Technique (CPT): An Advanced DInSAR Technique for Nonlinear Deformation Monitoring," Pure Appl. Geophys., No. 165, pp. 1167-1194, 2008.

[2] A. Ferretti, C. Prati, F. Rocca, “Permanent scatterers in SAR interferometry”, IEEE Trans. on Geoscience and Remote Sensing, Vol. 39, No 1, pp. 8-30, 2001.

[3] P. Berardino, G. Fornaro, R. Lanari, E. Sansosti, “A New Algorithm for Surface Deformation Monitoring Based on Small Baseline Differential Interferograms”, IEEE Trans. on Geoscience and Remote Sensing, Vol. 40, No. 11, pp. 2375-2383, 2002.

[4] Mora,O., Arbiol,R., Palà,V, “ICC’s Project for DInSAR Terrain Subsidence Monitoring of the Catalonian Territory”, Proceedings of IGARSS 2007,Barcelona.